



Design of a facile fluorescent probe with a large Stokes shift for hydrogen peroxide imaging in vitro and in vivo

Peng Hou^{a,*}, Song Chen^a, Guilin Liang^b, Hongmei Li^a, Hongguang Zhang^a

^a College of Pharmacy, Qiqihar Medical University, Qiqihar, Heilongjiang 161006, PR China

^b Department of Pharmacy, Qiqihar First Hospital, Qiqihar, Heilongjiang 161005, PR China

ARTICLE INFO

Article history:

Received 20 January 2020

Received in revised form 31 March 2020

Accepted 2 April 2020

Available online 3 April 2020

Keywords:

Hydrogen peroxide

Facile

A large Stokes shift

Cell imaging

ABSTRACT

By modifying 4'-hydroxybiphenyl-4-carbonitrile (**BPN-OH**) with 2-(4-(bromo-methyl)phenyl)-4,4,5,5-tetramethyl-1,3,2-dioxaborolane group, a facile fluorescent probe, **BPN-TOB**, for sensitively tracing H₂O₂ was designed and synthesized. **BPN-TOB** displayed a low detection limit (67 nM), fast response time (10 min), low cytotoxicity, a mega Stokes shift (170 nm) and a remarkable fluorescence enhancement (72-fold) in the detection of H₂O₂. Additionally, probe **BPN-TOB** could monitor exogenous and endogenous H₂O₂ in living MGC-803 cells (human gastric cancer cells) and RAW264.7 cells (leukemia cellsin mouse macrophage). In particular, this probe **BPN-TOB** was successfully utilized for imaging H₂O₂ in zebrafish.

© 2020 Elsevier B.V. All rights reserved.

1. Introduction

Hydrogen peroxide (H₂O₂) is an important physiologically active oxygen molecule, which plays a critical role in homeostasis and cellular signal transduction [1,2]. The endogenous H₂O₂ is mainly produced from cell respiration and peroxidation reaction regulated by a series of free radical scavenging enzymes. H₂O₂ is increasingly recognized as a marker of oxidative stress in living organisms [3]. However, the aberrant production of H₂O₂ within cellular mitochondria can lead to oxidative stress and the subsequent functional decline of organ systems [4,5]. Emerging evidences show that the abnormal expression of hydrogen peroxide is closely connected to various human diseases, such as neurodegenerative Alzheimer's, cardiovascular disorders and cancer [6–8]. Despite its significance, the precise mechanisms of H₂O₂ in physiological and pathological process still remain insufficiently understood. Therefore, the development of efficient and reliable H₂O₂ measurements in eukaryotic organisms is essential to elucidate its biological functions.

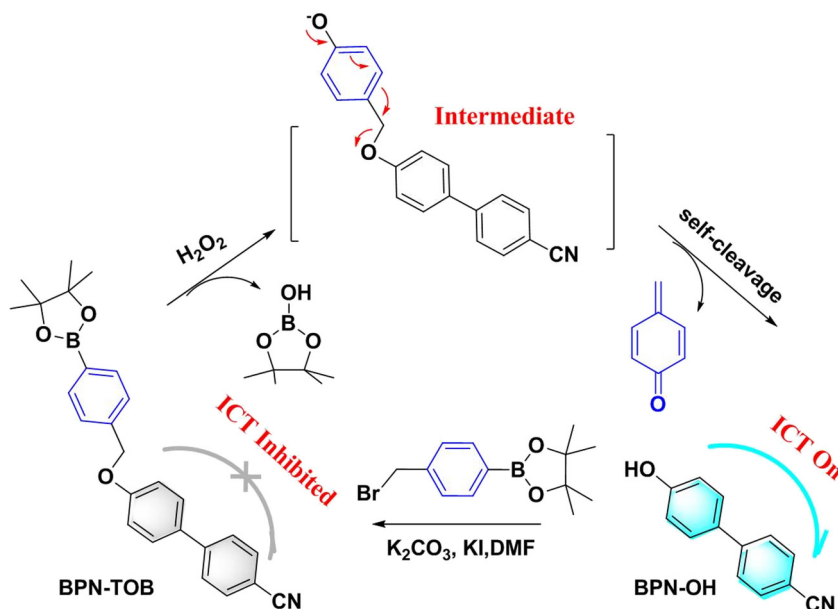
Till now, some approaches have been reported for H₂O₂ assay, including chemiluminescence, electrochemical, absorption and fluorescent sensors. Among these functional analytical methods [9–12], fluorescent probes have drawn significant interests because of their ease of use, inexpensiveness, high sensitivity, short response time,

high spatiotemporal resolution and less cell damage [13–16]. Hitherto, a batch of fluorescent probes with high sensitivity and excellent selectivity has been applied to monitor H₂O₂ in living systems based on specific detection strategies of H₂O₂ with various response sites [17–26], including benzyl, peroxalates, arylsulfonyl esters and boronic esters. However, some fluorescent probes toward H₂O₂ still have much room for improvement, such as small Stokes shift, slow response time and complicated synthesis procedures. Thus, developing a facile fluorescent probe with large Stokes shift and fast response time for sensitively identifying of H₂O₂ in vitro and *in vivo* is highly desirable.

Due to its excellent push-pull electronic system, a large Stokes shift induced by an intramolecular charge transfer process (ICT), valuable photostability and emission in the cyan region, 4'-hydroxybiphenyl-4-carbonitrile (**BPN-OH**) is an ideal candidate for the design of fluorescent sensors. Bearing the above factors, we herein present a facile fluorescent probe **BPN-TOB** with fast response time and large Stokes shift for sensitively tracing H₂O₂ by modifying **BPN-OH** with 2-(4-(bromomethyl)phenyl)-4,4,5,5-tetramethyl-1,3,2-dioxaborolane group (Scheme 1). In probe **BPN-TOB**, the ICT process is blocked by benzyl boronic pinacol ester protection. However, upon the addition of H₂O₂, **BPN-TOB** can be quickly converted into **BPN-OH**. Therefore, the ICT process from hydroxyl to cyano moiety in probe **BPN-TOB** was restored along with a significant cyan fluorescence response. Additionally, probe **BPN-TOB** could monitor exogenous and endogenous H₂O₂ in living MGC-803 cells (human gastric cancer cells) and RAW264.7 cells (leukemia cellsin mouse macrophage). Furthermore, this probe **BPN-TOB** was successfully utilized for imaging H₂O₂ in zebrafish.

* Corresponding author.

E-mail address: penghou@csu.edu.cn (P. Hou).



Scheme 1. Synthetic route to BPN-TOB and the sensing reaction with H₂O₂.

2. Experiment

2.1. Spectral measurements

The stock solution of probe **BPN-TOB** (1.0 mM) was appropriately dissolved in dimethyl sulfoxide. Mix the diluted stock solution of **BPN-TOB** and various-concentrations H₂O₂ (or other analytes) in pH 7.4 PBS (containing 1.0 mM CTAB) buffer solution. The final volume of test solution was adjusted to 3 mL by ultrapure water. When the test solution was shaken well for 10 min under room temperature, the fluorescence measurement of mixture solution was conducted with slit widths of 5.0/5.0 nm.

2.2. Cell culture and fluorescence imaging experiments

Before the fluorescence imaging, the MGC-803 cells and RAW264.7 cells were plated on culture dishes and grown in Dulbecco's modified Eagle's medium (at 37 °C and 5% CO₂) for 24 h. For MGC-803 cells exogenous H₂O₂ imaging: after washed the medium with PBS, MGC-803 cells were stained with **BPN-TOB** (10.0 μM) for 30 min, incubated with different concentrations (20.0 μM, 50.0 μM, 100.0 μM) H₂O₂ for another 30 min, and imaged subsequent to washed three times with PBS. While the other MGC-803 cells were only incubated with **BPN-TOB** (10.0 μM) for 30 min, and these fluorescence imaging of intracellular H₂O₂ was performed on Zeiss LSM710 microscope. For RAW264.7 cells endogenous H₂O₂ imaging: when got rid of the medium with PBS, RAW264.7 cells were stimulated with (2.0 μg/mL) PMA and added with **BPN-TOB** (10.0 μM). The obtained imaging was compared with the imaging of RAW264.7 cells incubated with **BPN-TOB** + H₂O₂ and only **BPN-TOB**. Meanwhile, the other stimulated RAW264.7 cells were precultured with 1.0 mM *N*-acetyl-L-cysteine (NAC), which was considered as a common inhibitor, and cultured with **BPN-TOB** (10.0 μM), then subjected to remove the residual solution with PBS, confocal fluorescence imaging was carried out.

2.3. Zebrafish imaging

By using confocal microscope, the zebrafish imagings were performed after removed and washed the different solvent with the PBS

buffer. The zebrafish were incubated at 28 °C on a light and dark cycle (13/11 h). The 4-day-old zebrafish were raised in E2 embryo media. For the image, zebrafish were pre-maintained in H₂O₂ (100.0 μM) for 30 min, and then treated with **BPN-TOB** (10.0 μM) for another 30 min. In the control group, zebrafish were only incubated with **BPN-TOB** (10.0 μM) for 30 min.

2.4. Apparatus and reagents

Cell imaging, NMR spectra, pH measurements and mass spectrometric experiments were conducted on Zeiss LSM710 microscope, BRUKER 600 spectrometer, PHS-3C pH meter, Waters® Xevo G2-S QToF™ mass spectrometer, respectively. The emission spectra and UV-Vis spectra were carried out with a Shimadzu RF5301PC spectrophotometer and a Shimadzu UV-2450 spectrophotometer. The slit widths of emission and excitation were 5.0 nm. All reagents for preparation of **BPN-TOB** were commercially available and not further purified to use.

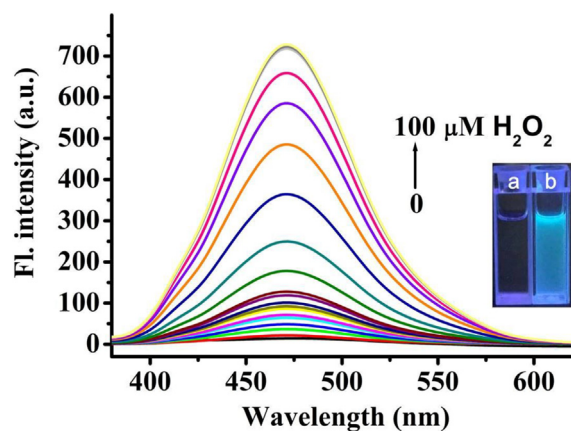


Fig. 1. Fluorescence spectral changes of **BPN-TOB** (10.0 μM) reacted with H₂O₂ (0.0–100.0 μM) in PBS buffer. Inset: fluorescence images of **BPN-TOB** (10.0 μM) in the absence (a) and presences (b) of H₂O₂ (100.0 μM) under a handheld 365 nm UV lamp.

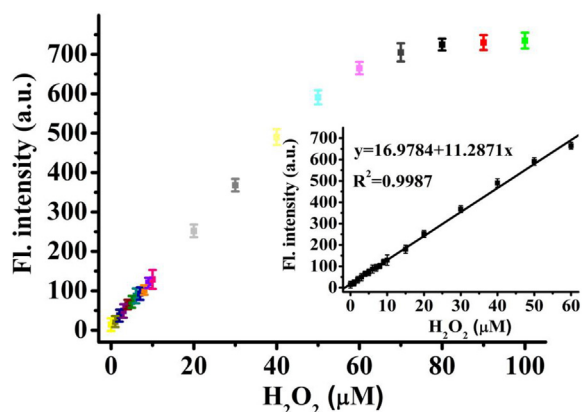


Fig. 2. Fluorescence intensity of **BPN-TOB** (10.0 μM) at 471 nm with the reaction of H_2O_2 concentration (0.0–100.0 μM) in PBS buffer. Inset: the plot of fluorescence intensity vs low concentrations of H_2O_2 .

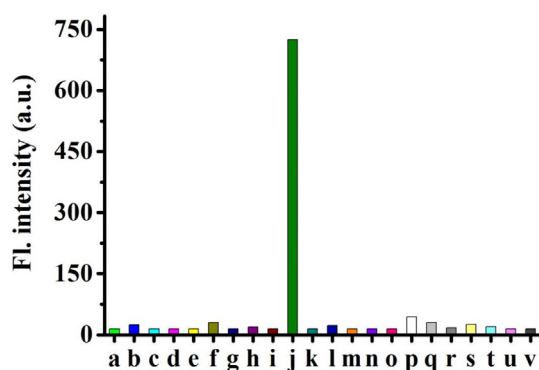


Fig. 3. The selectivity at 471 nm of **BPN-TOB** (10.0 μM) with the reaction of the various analytes (a–v: 100.0 μM for PO_4^{3-} , NO_2^- , $\text{S}_2\text{O}_3^{2-}$, SCN^- , I^- , ClO^- , F^- , NO_3^- , CO_3^{2-} , H_2O_2 , SO_3^{2-} , CN^- , Fe^{2+} , Ca^{2+} , Fe^{3+} , TBHP, $\bullet\text{OtBu}$, O^{2-} , ONOO^- , $\bullet\text{OH}$, GSH and Hcy).

2.5. Synthesis of probe **BPN-TOB**

BPN-OH (58.6 mg, 0.30 mmol), 2-(4-(bromomethyl)phenyl)-4,4,5,5-tetramethyl-1,3,2-dioxaborolane (128.2 mg, 0.6 mmol), KI

(8 mg) and K_2CO_3 (82.9 mg, 0.6 mmol) were dissolved in a solution of DMF (7 mL). The resulting mixture was stirred at 70 $^\circ\text{C}$ under argon atmosphere for 3 h. The reaction mixture was poured in 15 mL water and extracted with dichloromethane three times (8 mL \times 3). The organic layers were collected and dried over anhydrous sodium sulfate. The solvent was removed under vacuum and the residue was purified by silica gel column chromatography (eluent: dichloromethane) to afford probe **BPN-TOB** (yield 73%). ^1H NMR (600 MHz, $\text{DMSO}-d_6$) δ 7.88 (d, J = 8.3 Hz, 2H), 7.84 (d, J = 8.2 Hz, 2H), 7.75–7.67 (m, 4H), 7.48 (d, J = 7.6 Hz, 2H), 7.13 (d, J = 8.6 Hz, 2H), 5.23 (s, 2H), 1.29 (s, 12H). ^{13}C NMR (150 MHz, $\text{DMSO}-d_6$) δ 159.33, 144.66, 140.81, 135.07, 133.26, 131.18, 128.33, 127.37, 127.26, 119.47, 116.00, 109.66, 84.16, 69.55, 25.15. HRMS (EI) m/z calcd for $[\text{C}_{26}\text{H}_{26}\text{BNO}_3 + \text{Na}]^+$: 434.1903, Found: 434.1898.

3. Results and discussion

3.1. Sensing properties of probe **BPN-TOB** to H_2O_2

As illustrated in Fig. 1, the sensing ability of **BPN-TOB** toward various concentrations of H_2O_2 by fluorescence spectra in pH 7.4 buffer solutions (1.0 mM CTAB) was investigated. Probe **BPN-TOB** itself (10.0 μM) showed nearly no fluorescence at 471 nm because of the inhibited ICT process leading to the fluorescence quenching (Fig. S1). Nevertheless, upon treatment with H_2O_2 (0.0–100.0 μM), the emission peak of **BPN-TOB** at 471 nm evidently increased. Meanwhile, the emission intensity at 471 nm reached a plateau with 72-fold fluorescence enhancement in the presence of H_2O_2 . Notably, probe **BPN-TOB** displayed a large Stokes shift (170 nm) in response to H_2O_2 (Fig. S2), which can significantly reduce the self-quenching and auto-fluorescence [27–31]. Moreover, the emission intensity enhancement at 471 nm (Fig. 2) had an excellent relationship ($y = 16.9784 + 11.2871x$, $R^2 = 0.9987$) with H_2O_2 addition (0.0–60.0 μM). Based on signal-to-noise ratio of 3, the limit of detection of **BPN-TOB** for H_2O_2 was calculated to be 67 nM [32]. The above results implied that **BPN-TOB** is able to monitor H_2O_2 with good sensitivity.

3.2. Selectivity of probe **BPN-TOB**

The selectivity is a crucial evaluation criterion in identifying the practical ability of **BPN-TOB** toward H_2O_2 in living systems. Spectrometric methods were used to explore the probe optical properties over various biological agents and other similar ROS (100.0 μM) (including

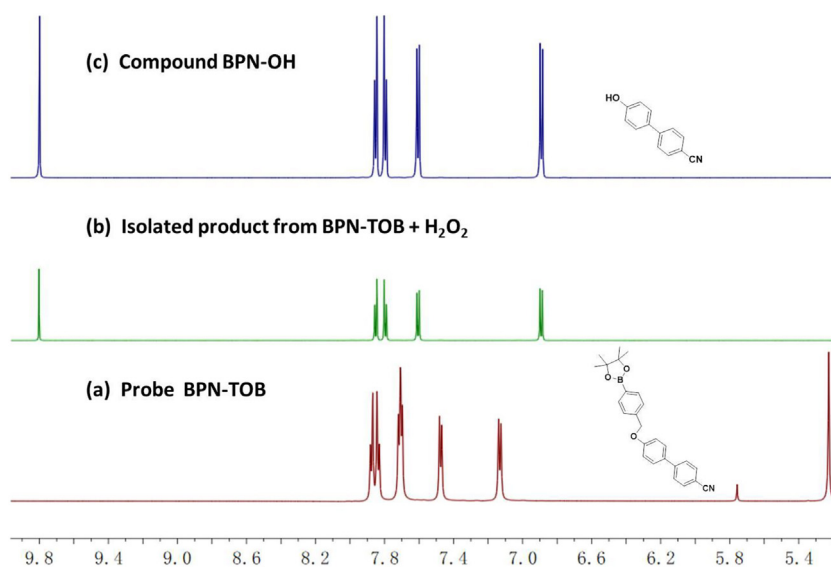


Fig. 4. Partial ^1H NMR spectroscopy of **BPN-TOB** (a), the isolated fluorescent product of **BPN-TOB** with H_2O_2 (b), and **BPN-OH** (c) in $\text{DMSO}-d_6$.

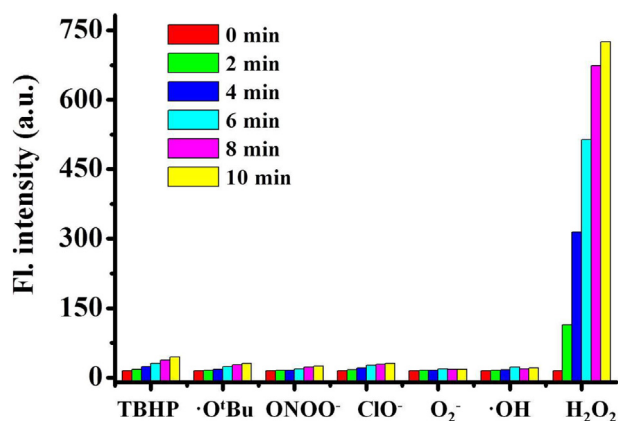


Fig. 5. Relative changes in fluorescence intensity of **BPN-TOB** upon the addition of H_2O_2 and other biologically ROS in different times, respectively.

PO_4^{3-} , NO_2^- , $\text{S}_2\text{O}_3^{2-}$, SCN^- , I^- , ClO^- , F^- , NO_3^- , CO_3^{2-} , SO_3^{2-} , CN^- , Fe^{2+} , Ca^{2+} , Fe^{3+} , TBHP, $\cdot\text{O}^t\text{Bu}$, O^{2-} , ONOO^- , $\cdot\text{OH}$, GSH and Hcy). As expected, the change in the fluorescence profiles of **BPN-TOB** ($10.0 \mu\text{M}$) revealed that a clear response was detected at 471 nm with only the addition of

H_2O_2 ($100.0 \mu\text{M}$). Other analytes did not induce discernible increase in the fluorescence intensity of **BPN-TOB** (Fig. 3). Meanwhile, to further investigate the interference of coexistence on the recognition of H_2O_2 by **BPN-TOB**, competitive studies were performed by fluorimetry. As shown in Fig. S3, the strong fluorescence enhancement of **BPN-TOB** ($10.0 \mu\text{M}$) by H_2O_2 with other coexistence ($100.0 \mu\text{M}$) was similar to that caused by H_2O_2 alone. The above experiments results confirmed that **BPN-TOB** had a specific response to H_2O_2 over other analytes.

3.3. Proposed mechanism

We hypothesized that the drastic fluorescence changes of **BPN-TOB** toward H_2O_2 was ascribed to the oxidation reaction of H_2O_2 with the boronate moiety in **BPN-TOB** and 1,6-rearrangement elimination reaction to generate **BPN-OH**, which restored the ICT process [33,34]. To confirm the above assumption, we decided to characterize the fluorescent product of **BPN-TOB** with H_2O_2 . Clearly, the fluorescent product of **BPN-TOB** with H_2O_2 displayed a quite similar ^1H NMR spectrum to that of **BPN-OH** (Fig. 4). Compared with the ^1H NMR spectrum of **BPN-TOB**, the peak signalling at 5.23 ppm assigned to the benzyl moiety in **BPN-TOB**, disappeared in the ^1H NMR spectrum of the fluorescent product of **BPN-TOB** with H_2O_2 . Meanwhile, a new peak signalling at 9.80 ppm assigned to the phenolic OH moiety was emerged. Moreover,

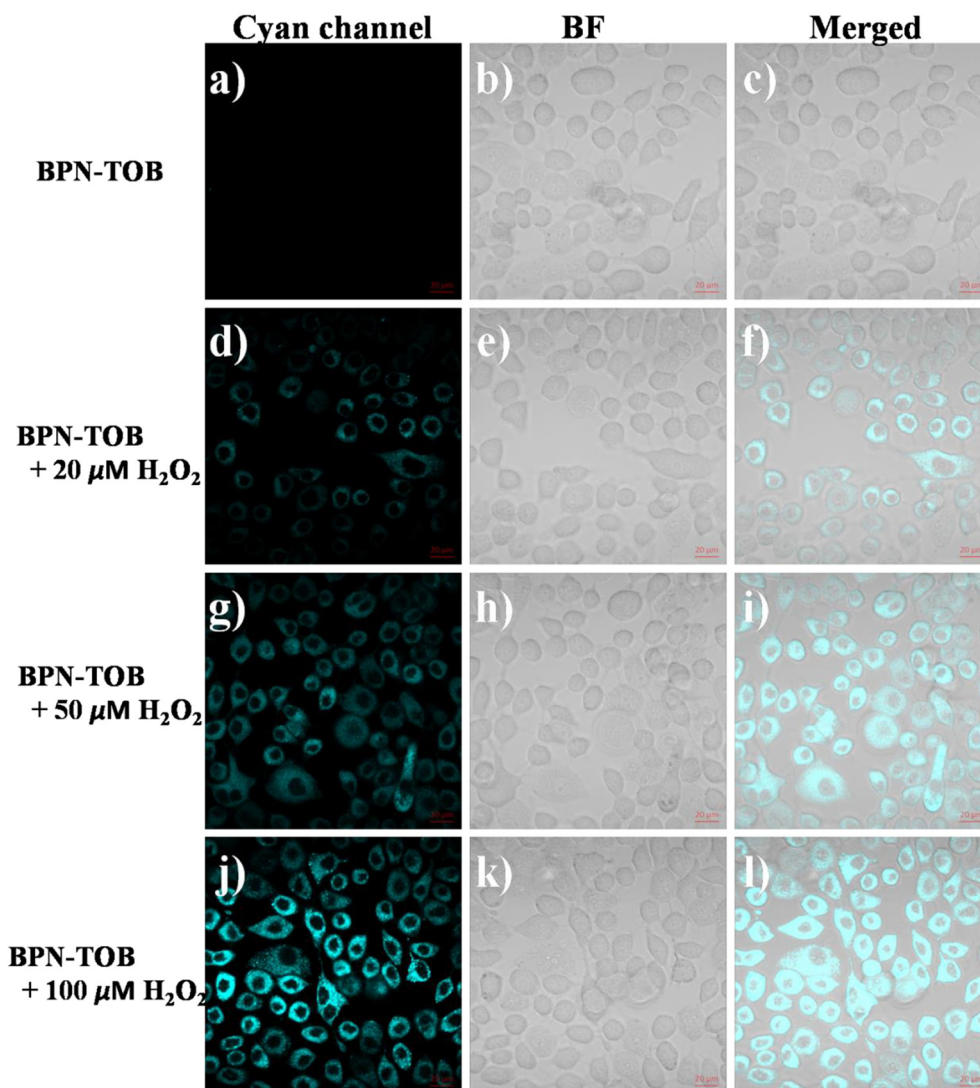


Fig. 6. Confocal fluorescence images of MGC-803 cells: Conditions: probe-stained cells were incubated with H_2O_2 of varying concentrations ($0.0 \mu\text{M}$, $20.0 \mu\text{M}$, $50.0 \mu\text{M}$ and $100.0 \mu\text{M}$). 30 min later, fluorescence imaging was performed.

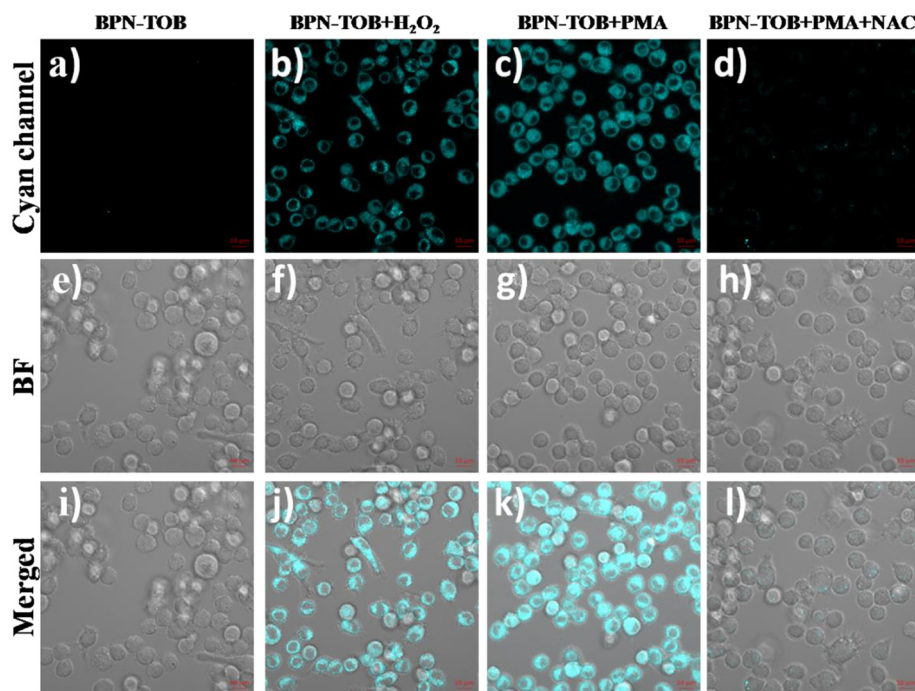


Fig. 7. Confocal fluorescence images of RAW264.7 cells exposed to only the probe **BPN-TOB** (a, e, i); the **BPN-TOB**-preloaded and then treated with H_2O_2 (b, f, j); the probe **BPN-TOB** after PMA stimulation (c, g, k); the probe **BPN-TOB** after PMA stimulation and treated with NAC (d, h, l).

the sensing mechanism in this article was also verified by HRMS analysis (Fig. S10). As expected, the fluorescent product of **BPN-TOB** with H_2O_2 (a peak at $m/z = 194.0599$) and **BPN-OH** $[M-H]^+$ (cal. 194.0606) nearly had the same molecular weight. The above HRMS and 1H NMR spectrum results strongly support the proposed sensing mechanism in Scheme 1.

3.4. Response time

For practical applications, it is needed to assess the ability of real-time and specific detection of **BPN-TOB** toward H_2O_2 . Compared with various ROS (TBHP, $\bullet OtBu$, $ONOO^-$, ClO^- , O^{2-} , $\bullet OH$), the time-dependent fluorescence intensity at 471 nm of **BPN-TOB** (10.0 μM) toward H_2O_2 (100.0 μM) was investigated. As manifested in Fig. S4, **BPN-TOB** itself was stable in the detection system of 7.4 PBS (containing 1 mM CTAB), **BPN-TOB** positive reacted with H_2O_2 immediately and reached a plateau within 10 min. The fluorescence intensity at 471 nm enhanced higher noticeably over the other similar ROS in Fig. 5. The result indicated that **BPN-TOB** is sufficiently stable for serving as a real-time monitoring agent for H_2O_2 detection over other ROS.

3.5. pH dependence of probe BPN-TOB

In consideration of pH-effect on the fluorescence detection of **BPN-TOB** toward H_2O_2 , the experiment of different pH conditions were executed in detail. The results exhibited that acid condition renders the probe **BPN-TOB** (10.0 μM) insensitive toward H_2O_2 (100.0 μM) detection (Fig. S5). However, the fluorescence enhancement of **BPN-TOB** response to H_2O_2 is considerably and sustained stability with an increase pH rang of 7.0–12.0. These results indicated that **BPN-TOB** possessed broad adaptability to discriminate H_2O_2 in complicated biosystems.

3.6. Fluorescent imaging of exogenous and endogenous H_2O_2 in cells

Encouraged by the above desirable performance of **BPN-TOB** in vitro optical response to H_2O_2 , we are become highly curious about the practicability of H_2O_2 -responsive in living cells. Firstly, the biocompatibility and cytotoxicity of **BPN-TOB** was evaluated by a MTT assay. The

experimental results showed that the cell viability of RAW264.7 cells and MGC-803 cells was greater than 93% overnight (Fig. S6), indicating that the concentration (1.0 μM , 2.0 μM , 5.0 μM , 10.0 μM , 20.0 μM) of **BPN-TOB** was safely and nontoxicity employed to visualize H_2O_2 in cells and animals. Then, the exogenous H_2O_2 imaging was proceeded to conduct in MGC-803 cells. As shown in Fig. 6, very weak intracellular cyan fluorescence was observed when **BPN-TOB** (10.0 μM) alone diffused into MGC-803 cells. In contrast, the incubation of H_2O_2 at different concentrations (20.0 μM , 50.0 μM , 100.0 μM) following the staining of the probe **BPN-TOB** individually, the intense cyan fluorescence was easily detected.

To further examine the capable of **BPN-TOB** visualizing endogenous in RAW264.7 cells, we applied RAW264.7 cells loaded the probe **BPN-TOB** to monitoring endogenous H_2O_2 with the stimulation of PMA. As shown in Fig. 7, the RAW264.7 cells only stained with **BPN-TOB** (10.0 μM) displayed a very faint fluorescence. After RAW264.7 cells were further incubated with H_2O_2 (100.0 μM), the cyan fluorescence became prominent (Fig. 7b, f and j). However, notable cyan increase fluorescence was observed in the cells stimulated by (2 $\mu g/mL$) PMA (Fig. 7c, g and k). To confirm the change in fluorescence intensity caused by the

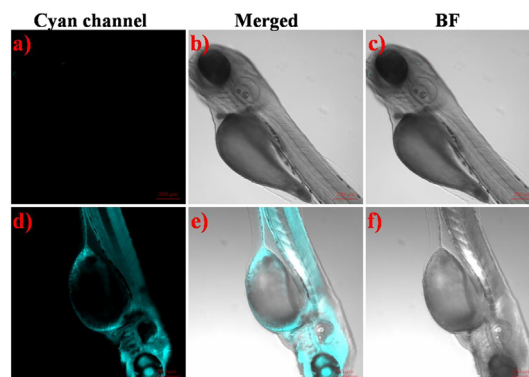


Fig. 8. Fluorescence (a, d), merged (b, e) and bright field (c, f) images of zebrafish. Top row (a–c): only seeded with probe **BPN-TOB** for 30 min. Bottom row (d–f): pre-trained with H_2O_2 for 30 min and then seeded with probe **BPN-TOB** for 30 min.

treatment of PMA in cells, the stimulated cells were treated with an antioxidant (1.0 mM, NAC) to eliminate H₂O₂ prior to **BPN-TOB** in cells. In this case, the fluorescence intensity of the cells was almost completely suppressed result from distinctly inhibited by NAC (Fig. 7d, h and l). Taken all results together, it is clearly indicated that **BPN-TOB** is capable of responding and visualizing the endogenous and exogenous H₂O₂ in living cells.

3.7. Fluorescence imaging in zebrafish

In view of the above satisfactory data of **BPN-TOB** for H₂O₂ in cellular-imaging studies, we next investigated the feasibility of **BPN-TOB** to trace H₂O₂ in zebrafish. As displayed in Fig. 8, negligible fluorescence in cyan channel was observed when zebrafish were incubated with **BPN-TOB** (10.0 μM) for 30 min. However, an intense cyan signal fluorescence was acquired in zebrafish imaging (Fig. 8d–f) when H₂O₂-pretreated (100.0 μM) zebrafish that were incubated in **BPN-TOB** for another 30 min. These zebrafish imaging data indicated that **BPN-TOB** could report H₂O₂ in zebrafish with excellent performance.

4. Conclusions

In conclusion, we designed and synthesized a facile fluorescent probe **BPN-TOB** using **BPN-OH** as the fluorophore and benzyl boronic pinacol ester as the recognition site for sensitively tracing H₂O₂. Probe **BPN-TOB** owned the advantages of a low detection limit (67 nM), fast response time (10 min), low cytotoxicity, a mega Stokes shift (170 nm) and a remarkable fluorescence enhancement (72-fold). Most importantly, probe **BPN-TOB** could monitor exogenous and endogenous H₂O₂ in vitro and in vivo with good performance.

CRedit authorship contribution statement

Peng Hou: Writing - original draft, Writing - review & editing. **Song Chen:** Methodology, Data curation. **Guilin Liang:** Visualization, Investigation. **Hongmei Li:** Software. **Hongguang Zhang:** Validation.

Acknowledgments

We are grateful to the Heilongjiang Provincial Department of Education Science and Technology Research Project, China (No. 2018-KYYWF-0098) for support.

Declaration of competing interest

The authors declare that they have no known competing financial interests or personal relationships that could have appeared to influence the work reported in this paper.

Appendix A. Supplementary data

Supplementary data to this article can be found online at <https://doi.org/10.1016/j.saa.2020.118338>.

References

- [1] S. Tomoyuki, K. Shuji, *Biochim. Biophys. Acta* 1832 (2013) 1362–1370.
- [2] S.G. Rhee, S.W. Kang, W. Jeong, T.S. Chang, K.S. Yang, H.A. Woo, *Curr. Opin. Cell Biol.* 17 (2005) 183–189.
- [3] P.D. Ray, B.W. Huang, Y. Tsuji, *Cell. Signal.* 24 (2012) 981–990.
- [4] R. Carnevale, C. Nocella, P. Pignatelli, S. Bartimocchia, L. Stefanini, S. Basili, M. Novo, A. D'Amico, V. Cammisotto, D. Pastori, F. Violi, *Atherosclerosis* 274 (2018) 29–34.
- [5] E. Murphy, A.J. Friedman, *J. Am. Acad. Dermatol.* 81 (2019) 1379–1386.
- [6] S. Mori, K. Morihito, T. Okuda, Y. Kasahara, S. Obika, *Chem. Sci.* 9 (2018) 1112–1118.
- [7] T. Finkel, M. Serrano, M.A. Blasco, *Nature* 448 (2007) 767–774.
- [8] M. Reth, *Nat. Immunol.* 3 (2002) 1129–1134.
- [9] Y. Hu, Z. Zhang, C. Yang, *Anal. Sci.* 24 (2008) 201–205.
- [10] A.K.M. Kafi, G. Wu, A. Chen, *Biosens. Bioelectron.* 24 (2008) 566–571.
- [11] X. Cheng, L. Huang, X. Yang, A.A. Elzatahry, A. Alghamdi, Y. Deng, *J. Colloid Interface Sci.* 535 (2018) 425–435.
- [12] X.L. Hao, Z.J. Guo, C. Zhang, A.M. Ren, *Phys. Chem. Chem. Phys.* 21 (2018) 281–291.
- [13] Y.Q. Hao, S. Chen, Y.L. Zhou, Y.T. Zhang, M.T. Xu, *Nanomaterials* 9 (2019) 974.
- [14] H. Zhang, L.Z. Xu, W.Q. Chen, J. Huang, C.S. Huang, J.R. Sheng, X.Z. Song, *Anal. Chem.* 91 (2019) 1904–1911.
- [15] S. Chen, P. Hou, J. Sun, H. Wang, L. Liu, *Molecules* 24 (2019) 3328.
- [16] P. Hou, J. Sun, H. Wang, L. Liu, L. Zou, S. Chen, *Sens. Actuators B Chem.* 304 (2020), 127244.
- [17] M. Abo, Y. Urano, K. Hanaoka, T. Terai, T. Komatsu, T. Nagano, *J. Am. Chem. Soc.* 133 (2011) 10629–10637.
- [18] D. Srikun, A.E. Albers, C.I. Nam, A.T. Iavarone, C.J. Chang, *J. Am. Chem. Soc.* 132 (2010) 4455–4465.
- [19] L. Zhou, H. Ding, W. Zhao, S. Hu, *Spectrochim. Acta A Mol. Biomol. Spectrosc.* 206 (2019) 529–534.
- [20] X. Liu, H. Tian, L. Yang, Y. Su, M. Guo, X. Song, *Sens. Actuators B Chem.* 255 (2018) 1160–1165.
- [21] N. Li, J. Huang, Q. Wang, Y. Gu, P. Wang, *Sens. Actuators B Chem.* 254 (2018) 411–416.
- [22] J. Liu, S. Zhou, J. Ren, C. Wu, Y. Zhao, *Analyst* 142 (2017) 4522–4528.
- [23] X. Liang, X. Xu, D. Qiao, Z. Yin, L. Shang, *Chem. Asian J.* 12 (2017) 3187–3194.
- [24] Q. Ma, X. Li, J. Zhang, X. Zhu, L. Zhou, H. Liu, *Anal. Methods* 9 (2017) 4558–4565.
- [25] Y. Lu, X. Shi, W. Fan, C.A. Black, Z. Lu, C. Fan, *Spectrochim. Acta A Mol. Biomol. Spectrosc.* 190 (2018) 353–359.
- [26] F. Xu, W. Tang, S. Kang, J. Song, X. Duan, *Dyes Pigments* 153 (2018) 61–66.
- [27] S. Chen, H.M. Li, P. Hou, *Anal. Chim. Acta* 993 (2017) 63–70.
- [28] S. Chen, H. Li, P. Hou, *Sens. Actuators B Chem.* 256 (2018) 1086–1092.
- [29] P. Hou, J. Wang, S. Fu, L. Liu, S. Chen, *Spectrochim. Acta A Mol. Biomol. Spectrosc.* 213 (2019) 342–346.
- [30] S. Chen, P. Hou, J. Wang, S. Fu, L. Liu, *J. Photoch. Photobiol. A Chem.* 363 (2018) 7–12.
- [31] S. Chen, P. Hou, J. Wang, S. Fu, L. Liu, *Anal. Bioanal. Chem.* 410 (2018) 4323–4330.
- [32] H. Irving, H. Freiser, T. West, Pergamon Press, Oxford, 1981.
- [33] X. Liu, L. He, L. Yang, Y. Geng, L. Yang, X. Song, *Sens. Actuators B Chem.* 259 (2018) 803–808.
- [34] L. Tang, M. Tian, H. Chen, X. Yan, K. Zhong, Y. Bian, *Dyes Pigments* 158 (2018) 482–489.